Research Square

Preprints are preliminary reports that have not undergone peer review.
They should not be considered conclusive, used to inform clinical practice,
or referenced by the media as validated information.

Soft-x-ray free-electron laser pulses stabilize a competing order in helimagnet

Haichao Xu

xuhaichao@fudan.edu.cn

Fudan University https://orcid.org/0000-0003-4852-0470

Jiahao Ye

Laboratory of Advanced Materials, State Key Laboratory of Surface Physics, and Department of Physics, Fudan University

Qi Jiang

Shanghai Advanced Research Institute, Chinese Academy of Sciences

Zhitong An

Laboratory of Advanced Materials, State Key Laboratory of Surface Physics, and Department of Physics, Fudan University

Shenglin Tang

Laboratory of Advanced Materials, State Key Laboratory of Surface Physics, and Department of Physics, Fudan University

Xingtian Sun

Laboratory of Advanced Materials, State Key Laboratory of Surface Physics, and Department of Physics, Fudan University

Wenchang Hou

Center for Transformative Science，School of Physical Science and Technology, ShanghaiTech University

Yao Shen

Institute of Physics, Chinese Academy of Sciences https://orcid.org/0000-0003-4697-4719

Qinghua Zhang

Institute of Physics, Chinese Academy of Sciences https://orcid.org/0000-0001-9086-7000

Limin Zhou

Shanghai Advanced Research Institute, Chinese Academy of Sciences

Zhenhua Chen

Shanghai Advanced Research Institute, Chinese Academy of Sciences

Jun Zhao

Laboratory of Advanced Materials, State Key Laboratory of Surface Physics and Department of Physics

Rui Peng

Fudan University https://orcid.org/0000-0003-2507-4615

Mao Ye
Shanghai Advanced Research Institute, Chinese Academy of Sciences
Donglai Feng
New Cornerstone Science Laboratory, Hefei National Laboratory

Article

Keywords:

Posted Date: October 9th, 2026

DOI: https://doi.org/10.21203/rs.3.rs-11068927/v1

License: This work is licensed under a Creative Commons Attribution 4.0 International License.
Read Full License

Additional Declarations: There is no conflict of interest

Soft-x-ray free-electron laser pulses stabilize a competing order in helimagnet

Jiahao Ye[1#], Qi Jiang[2#], Zhitong An[1], Shenglin Tang[1], Xingtian Sun[1], Wenchang Hou[3], Yao Shen[1,4], Qinghua Zhang[4], Limin Zhou[2], Zhenhua Chen[2], Jun Zhao[1], Rui Peng[1,5], Mao Ye[2,*], Haichao Xu[1,5,*], Donglai Feng[6,*]

[1]Laboratory of Advanced Materials, State Key Laboratory of Surface Physics, and Department of Physics, Fudan University, Shanghai 200438, China
[2]Shanghai Advanced Research Institute, Chinese Academy of Sciences, Shanghai 201204, China
[3]Center for Transformative Science, School of Physical Science and Technology, ShanghaiTech University, Shanghai, 201210, China
[4]Beijing National Laboratory for Condensed Matter Physics, Institute of Physics, Chinese Academy of Sciences Beijing 100190, China
[5]Shanghai Research Center for Quantum Sciences, Shanghai 201315, China
[6]New Cornerstone Science Laboratory, Hefei National Laboratory, Hefei 230026, China
[*]Corresponding authors: yem@sari.ac.cn; xuhaichao@fudan.edu.cn; dlfeng@hfnl.cn

(Dated: September 17, 2026)

Intense light pulses can drive quantum materials away from equilibrium and access states that are absent under ordinary conditions. Whether resonant soft-x-ray free-electron laser (XFEL) pulses can persistently modify an ordered phase, rather than merely probe or damage it, remains an important question. Here we show that soft-x-ray XFEL exposure stabilizes a short-range incommensurate order in the itinerant helimagnet CrAs. Pristine CrAs exhibits only the native helical magnetic reflection, whereas after XFEL irradiation a second Cr-resonant peak appears at a distinct wave vector and remains observable by synchrotron resonant soft-x-ray scattering. This induced order develops below $T^* \approx 230$ K, has a correlation length of approximately 4 nm, and exhibits polarization-dependent resonant scattering with a modified Cr 3*d* spectral fingerprint. X-ray absorption and electron microscopy show that the CrAs framework is largely preserved while the near-surface lattice environment is locally modified. Time-resolved measurements further show that the induced order is optically suppressible and recovers on a picosecond timescale. These results establish soft-x-ray FEL pulses as an active perturbation for selecting competing orders in fragile correlated magnets.

I. INTRODUCTION

Controlling quantum matter with light has become a central route for accessing states that are difficult to realize under equilibrium conditions. Ultrafast optical and terahertz fields can transiently reshape electronic, magnetic, orbital, and lattice degrees of freedom, giving rise to superconducting-like optical responses, coherent control of magnetic excitations, photoinduced phase transitions, and long-lived hidden states [1–6]. These advances establish light not only as a probe of quantum materials, but also as an active perturbation capable of reorganizing their energy landscapes.

X-ray free-electron lasers extend this concept to a distinct light–matter interaction regime. Their femtosecond duration and high peak brilliance enable ultrafast experiments with intense x-ray pulses, while resonant soft-x-ray scattering provides elemental selectivity and momentum resolution for tracking ordered states [7–10]. However, intense soft-x-ray pulses also deposit substantial energy into the near-surface region and may modify the local structural or electronic environment [11–13]. This dual role raises a basic question: can resonant soft-x-ray FEL exposure persistently stabilize an ordered state that is absent in the pristine material, rather than simply probe an existing order or produce featureless damage?

CrAs provides a sensitive platform for addressing this question. It hosts unconventional superconductivity and quantum criticality under pressure [14–19], which are believed to be closely related to its helical magnetism [20]. The incommensurate helical magnetism emerges at ambient pressure below $T_S \approx 268$ K, with a propagation vector along $(0, 0, L)$ [14, 17, 21–23]. The helical pitch and correlation length evolve strongly with temperature, reflecting a delicate balance among competing exchange interactions, Dzyaloshinskii–Moriya interactions, magnetic anisotropy, and magnetoelastic coupling [24, 25]. Such sensitivity makes CrAs an ideal system in which a local lattice perturbation introduced by intense soft-x-ray irradiation may select a competing magnetic or magnetoelastic configuration, as schematically illustrated in Figs. 1(a,b).

Here we show that intense soft-x-ray XFEL irradiation stabilizes a previously absent incommensurate order in CrAs. By combining synchrotron resonant soft-x-ray scattering (RSXS), x-ray absorption spectroscopy (XAS), scanning transmission electron microscope (STEM), and time-resolved RSXS at an XFEL facility, we show that the induced state is Cr-derived, short-ranged, optically suppressible, and distinct from the native helical magnetic order. The results reveal how resonant soft-x-ray pulses can locally modify the ordering landscape of a fragile correlated magnet and stabilize a competing order that is not realized in pristine CrAs.

II. RESULTS

A. XFEL-induced incommensurate order in CrAs

We first characterized the native helical magnetic order of pristine CrAs using synchrotron RSXS at the Cr L_3 edge. The measurements were performed at $T = 20$ K in the same $(0, 0, L)$ scattering geometry as in our previous study [25] [Fig. 1(a)]. In pristine CrAs without XFEL exposure, a helical magnetic reflection is observed at $\boldsymbol{q}_1 \approx (0, 0, 0.352)$ [Fig. 1(c)], consistent with previous reports [25]. This reflec-

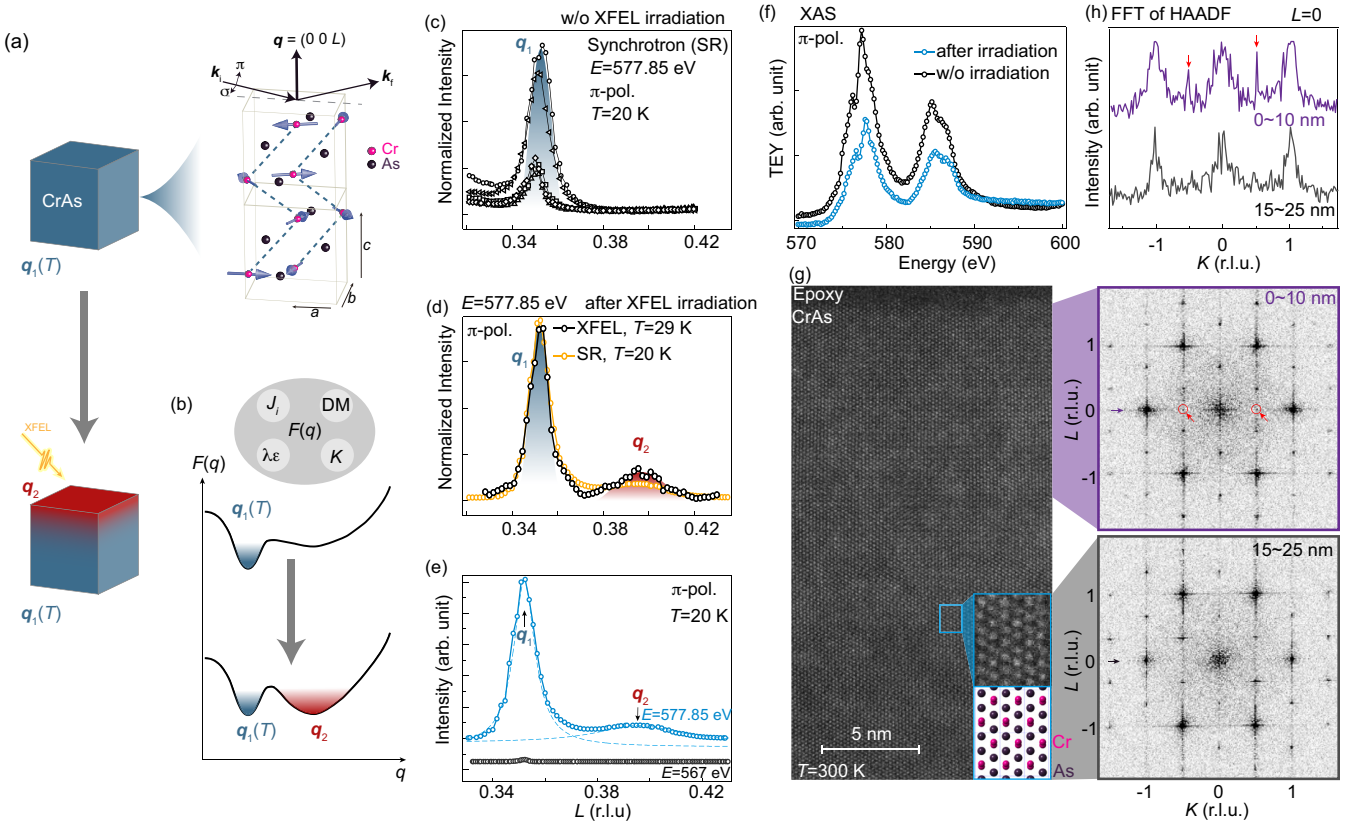


FIG. 1. **XFEL irradiation stabilizes a competing order in CrAs.** (a) Illustration of the helical spin order ($\boldsymbol{q}_1$) in CrAs, the RSXS scattering geometry, and the stabilization of an emergent order ($\boldsymbol{q}_2$) by XFEL irradiation. (b) Schematic ordering landscape $F(q)$ from the competing magnetic interactions and its modification by XFEL irradiation. The competing magnetic interactions may include the competing exchange interactions (J_i), Dzyaloshinskii-Moriya interactions (DM), magnetic anisotropy (K), and magnetoelastic coupling ($\lambda\epsilon$). The curves schematically represent the ordering tendency as a function of propagation vector and are not quantitative free-energy calculations. (c) L-scans measured with photons at the Cr L_3 resonance at various spots of pristine CrAs crystal without XFEL irradiation. (d) On-resonance L-scans measured at XFEL irradiated sample by XFEL and synchrotron (SR). (e) L-scans measured with π-polarized photons at the Cr L_3 resonance and at an off-resonant energy, normalized by the intensity of $\boldsymbol{q}_1$. (f) Cr L-edge XAS spectra measured before and after XFEL irradiation. (g) HAADF-STEM image of the irradiated near-surface region along [100] direction and corresponding FFTs from near-surface (0~10 nm) and bulk regions (15~25 nm). Red arrows mark additional spots in the near-surface FFT. (h) Line profiles of FFTs along L=0 to highlight the additional spots in the near-surface FFT.

tion is reproducibly detected at different positions on the pristine sample, while no additional ordered peak is observed at higher L=0.38–0.42 [Fig. 1(c)]. These measurements establish the equilibrium RSXS response of CrAs before irradiation.

We then exposed CrAs to intense XFEL pulses tuned near the Cr L_3 edge. The incident photon energy was 576 eV. After transmission through the downstream KB optics, the photon number at the sample was estimated to be 2.75×10^{10} photons per pulse, corresponding to a peak photon fluence of $5.2{\times}10^{14}$ photons cm^{-2} pulse^{-1} and a peak photon flux density of 2.1×10^{27} photons s^{-1} cm^{-2} (see Supplementary Section I). After approximately 1.2×10^4 pulses, an L-scan measured using the XFEL beam resolves not only the native helical reflection at $\boldsymbol{q}_1$, but also an additional incommensurate reflection at $\boldsymbol{q}_2 \approx (0, 0, 0.396)$ [Fig. 1(d)]. The emergence of this additional peak after XFEL exposure, together with its absence in pristine CrAs, identifies it as an irradiation-induced feature.

The induced $\boldsymbol{q}_2$ reflection persists after XFEL exposure and can be detected subsequently using synchrotron RSXS [Fig. 1(d)]. Both the native $\boldsymbol{q}_1$ reflection and the induced $\boldsymbol{q}_2$ reflection are strongly suppressed when the incident photon energy is tuned away from the Cr L_3 resonance to 567 eV [Fig. 1(e)]. This resonant behavior demonstrates that the induced peak is associated with Cr-derived electronic states rather than ordinary non-resonant structural scattering.

We next examined whether XFEL irradiation causes a large chemical or structural transformation. Cr L-edge XAS spectra measured before and after irradiation retain nearly identical peak positions and overall lineshapes [Fig. 1(f)], arguing against a substantial change in the average Cr valence or chemical composition. HAADF-STEM measurements near the irradiated region show that the CrAs lattice remains largely intact, without clear evidence for amorphization or secondary phases [left of Fig. 1(g)]. Nevertheless, the near-surface region within approximately 0 ~ 10 nm from the irradiated sur-

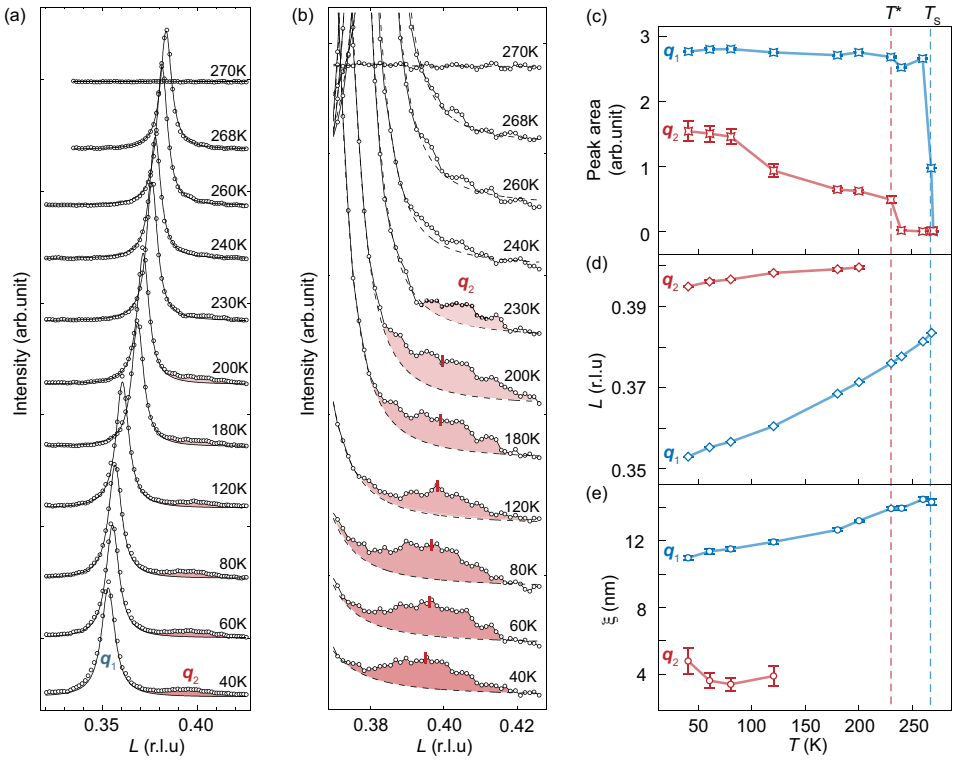


FIG. 2. **Temperature evolution of the native helical order q_1 and XFEL-induced order q_2.** (a) Temperature-dependent RSXS profiles along $(0, 0, L)$. (b) Enlarged view around the XFEL-induced reflection. (c–e) Integrated intensity, propagation vector, and correlation length of the two orders as functions of temperature, respectively.

face exhibits an additional periodic contrast modulation, as revealed by weak extra spots in the corresponding FFT [upper-right of Fig. 1(g) and Fig. 1(h)]. These extra FFT spots are absent in the deeper bulk-like region 15 $\sim$ 25 nm from the surface. The extra FFT spots occur near $K = \pm 0.5$ r.l.u., indicating an in-plane structural modulation distinct from the out-of-plane q_2 reflection detected by RSXS along $(0, 0, L)$. Taken together, the RSXS, XAS, and STEM results indicate that XFEL irradiation locally modifies the near-surface lattice environment without destroying the CrAs framework, thereby stabilizing a distinct Cr-derived incommensurate order.

B. Temperature evolution and short correlation length

In the temperature-dependent RSXS measurements performed using synchrotron radiation, the native q_1 peak displays the established behavior of CrAs: its propagation vector shifts from $L \approx 0.352$ to $L \approx 0.385$ upon warming and disappears at the helimagnetic transition temperature $T_S \approx 268$ K [Fig. 2(a,d)]. Meanwhile, its correlation length increases anomalously upon warming [Fig. 2(e)]. This counterintuitive behavior was reported in our previous study and attributed to the temperature-dependent evolution of the Dzyaloshinskii–Moriya interaction and defect-pinned helical domains [25]. It reflects the high sensitivity of the magnetic balance in CrAs to local perturbations.

By contrast, the XFEL-induced q_2 reflection shifts only slightly from $L \approx 0.396$ to $L \approx 0.401$ upon warming [Fig. 2(b,d)]. More importantly, its integrated intensity decreases systematically and becomes undetectable above $T^* \approx 230$ K, well below the T_S of q_1 [Fig. 2(c)]. The distinct propagation-vector evolution and separate characteristic temperature scale demonstrate that q_2 is not a static structural artifact or a fragmented component of the native helical order. Instead, it is an irradiation-stabilized order with its own thermal response.

The q_2 state is also substantially more short-ranged than the native helical order. Its correlation length, estimated from the inverse linewidth after converting the peak width into absolute momentum units, is approximately 4 nm along c axis, compared with 11 $\sim$ 14 nm for the native q_1 order [Fig. 2(e)]. Together with the near-surface structural modulation and spatial inhomogeneity shown in Fig. 1, this short correlation length is consistent with finite q_2-ordered domains forming within the XFEL-modified near-surface region, rather than a homogeneous bulk phase extending throughout the crystal.

C. Resonant and polarization-dependent character

Energy- and polarization-dependent RSXS measurements were conducted using synchrotron radiation. Both reflections exhibit pronounced resonant enhancement across the Cr $L_{2,3}$ edges, demonstrating their coupling to Cr-derived 3d electronic states [Fig. 3(a–d)]. Throughout the measured energy range, the q_2 reflection remains substantially broader along L [Fig. 3(c–d)] than the native helical peak [Fig. 3(a–b)], consistent with its shorter correlation length. For both orders, the scattering intensity is stronger for π-polarized than for σ-polarized incident photons [Figs. 3(e,f)]. For the native q_1 order, this polarization dependence is consistent with the expected resonant magnetic scattering response of the helical magnetic structure [25–28]. The qualitatively similar polar-

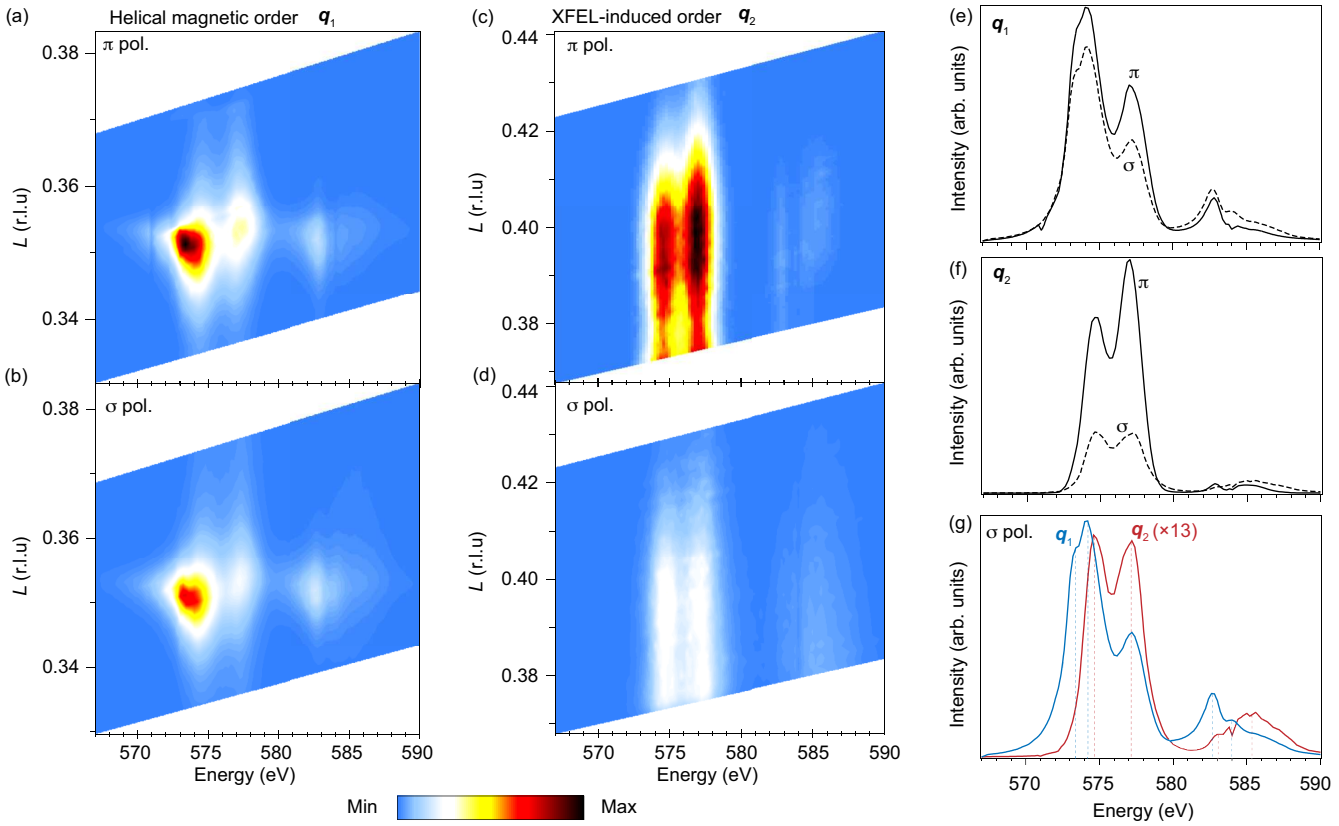


FIG. 3. **Resonant and polarization-dependent characterization of the native (q_1) and XFEL-induced (q_2) orders.** (a,b) Resonant profiles of the native helical order measured with π- and σ-polarized incident photons. (c,d) Corresponding resonant profiles of the XFEL-induced order. (e,f) Polarization-dependent integrated intensities of the two orders. (g) Incident-energy dependence of the integrated scattering intensities. For comparison of the line shapes, the q_2 profile is scaled by a constant factor. These measurements were conducted at T = 20 K.

ization dependence of the q_2 reflection therefore supports a substantial magnetic contribution to the induced order. However, the polarization contrast is considerably stronger for q_2 [Fig. 3(f)] than for q_1 [Fig. 3(e)]. Since the polarization dependence of resonant scattering is sensitive to the magnetic configuration, scattering geometry, and resonant tensor form factors, this difference indicates that the XFEL-induced state is not simply the native helical structure reproduced at a different propagation vector.

Both reflections show resonant features at the Cr L_3 and L_2 edges, but their spectral fingerprints are clearly different [Fig. 3(g)]. At the L_3 edge, the native q_1 order has its dominant spectral weight near 574 eV, whereas the main spectral weight of the XFEL-induced q_2 reflection is redistributed toward higher photon energies around 574.7 eV. In addition, the weaker q_1 feature near 577.2 eV is strongly enhanced in the q_2 spectrum. A similar redistribution is observed at the L_2 edge, where the dominant feature shifts from approximately 582.8 eV for q_1 to 585.3 eV for q_2. These changes in the resonant line shape suggest that the XFEL-induced state involves a modified local Cr 3d electronic environment compared with the native helimagnetic phase, possibly associated with changes in orbital occupation, hybridization, or crystal-field environment [29–31].

D. Ultrafast dynamics of the induced order

The nonequilibrium response of the XFEL-induced order was examined using time-resolved RSXS. In the pump–probe geometry, optical pump pulses with photon energy $h\nu$ = 1.55 eV and pulse duration Δt_{pump} = 82 fs were used to excite the sample, while soft-x-ray FEL probe pulses tuned to the Cr L_3 edge monitored the diffraction intensity [Fig. 4(a)]. The procedure used to extract normalized diffraction intensities in the presence of FEL shot-to-shot fluctuations in intensity and photon energy is described in Supplementary Sections I.C–I.E.

At T = 29 K, the diffraction intensity of the native helical magnetic order q_1 is suppressed by approximately 20% following near-infrared excitation with a fluence of 0.57 mJ cm^{-2} [Fig. 4(b)]. The subsequent intensity evolution is non-monotonic. Because the q_1 measurement is particularly sensitive to FEL photon-energy drift near the Cr L_3 resonance, as discussed in Supplementary Section I.E, the present data do not allow a reliable extraction of a quantitative intrinsic recovery timescale for the native helical order. Nevertheless, the q_1 trace demonstrates that the native order responds to optical excitation under the same pump–probe conditions.

The XFEL-induced q_2 order exhibits a reproducible pump-

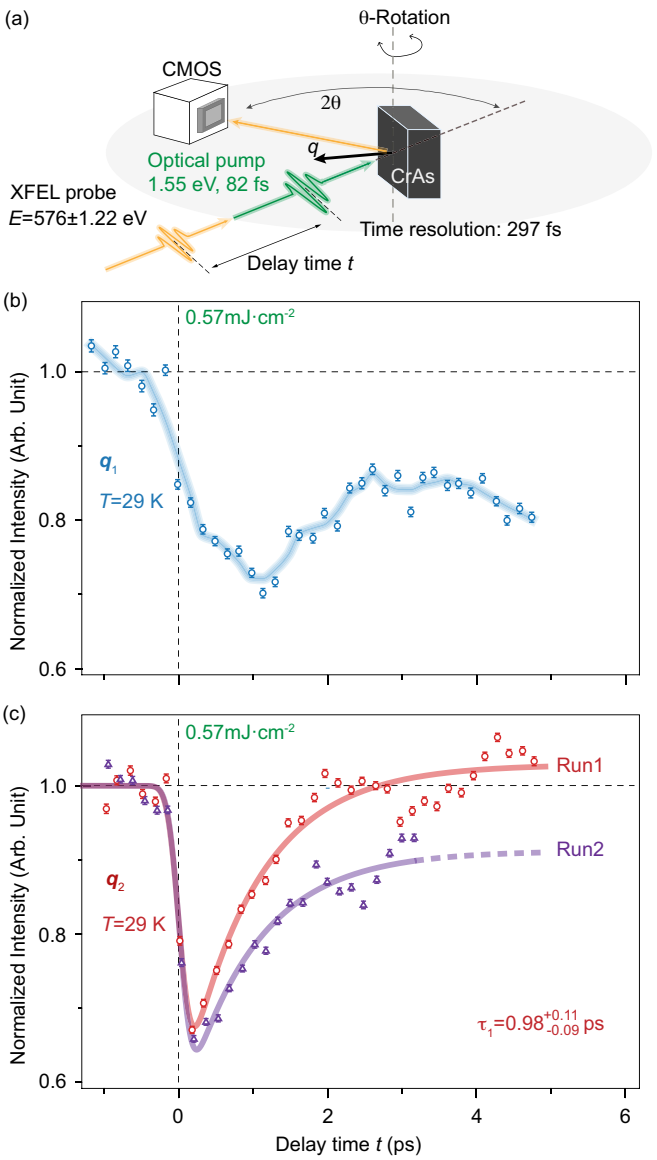


FIG. 4. **Time-resolved RSXS of the native helical order $\boldsymbol{q}_1$ and XFEL-induced order $\boldsymbol{q}_2$ in CrAs.** (a) Schematic pump-probe geometry. (b) Transient integrated intensity of the native helical order measured at $\boldsymbol{q}_1$. The blue curve is a guide to the eye. (c) Transient integrated intensities of the XFEL-induced order measured at $\boldsymbol{q}_2$ in two subsequent runs. The solid lines are fits incorporating the prompt suppression and fast recovery dynamics, with a constant accounts for the effect of photon energy drift and possible slow recovery processes. In (b) and (c), the error bars represent the conditional standard errors of the slopes obtained from linear fittings (Supplementary Section I.C).

induced suppression followed by recovery on a picosecond timescale [Fig. 4(c)]. Two consecutive measurements under nominally identical conditions show similar initial suppression and recovery dynamics, although their long-delay recovery levels differ. This difference is attributed mainly to slow drift of the FEL photon energy relative to the resonant condition, as analyzed in Supplementary Section I.E. The $\boldsymbol{q}_2$ traces were therefore fitted using a phenomenological recovery function convolved with the experimentally determined instrument response, with a constant term accounting for photon-energy drift and possible slow recovery components (Supplementary Section IV).

The fits yield a dominant recovery timescale of $\tau_1 = 0.98^{+0.11}_{-0.09}$ ps for the XFEL-induced $\boldsymbol{q}_2$ order. This fast recovery process is not clearly identified in $\boldsymbol{q}_1$, suggesting a distinct relaxation pathway of $\boldsymbol{q}_2$ with faster and simpler recovery dynamics. This picosecond timescale is comparable to ultrafast recovery processes reported for magnetically ordered correlated materials [32–35]. Together with the finite characteristic temperature and short correlation length described above, the reproducible optical suppression and recovery provide further evidence that the $\boldsymbol{q}_2$ reflection is associated with a collective ordered state rather than a static irradiation background.

III. DISCUSSION AND CONCLUSION

The present results identify the XFEL-induced $\boldsymbol{q}_2$ reflection as a distinct Cr-derived order stabilized in the irradiated region of CrAs. Its emergence can be understood from the delicate magnetic balance of this helimagnet. In pristine CrAs, the native $\boldsymbol{q}_1$ helix is selected by competing exchange interactions, Dzyaloshinskii–Moriya interactions, magnetic anisotropy, and magnetoelastic coupling; this balance is reflected by the strong temperature dependence of the helical pitch and correlation length [25]. XFEL irradiation locally modifies the near-surface lattice environment while largely preserving the CrAs framework. Such a local perturbation can shift the balance among competing interactions and select a nearby magnetic or magnetoelastic configuration [Figs. 1(a,b)]. In this picture, the $\boldsymbol{q}_2$ state is not a random damage feature, but a short-range order selected by an irradiation-modified interaction landscape.

Beyond CrAs, our results highlight a broader aspect of light–matter interaction at next-generation x-ray facilities. XFEL pulses are usually treated as ultrabright probes whose radiation damage must be minimized [8, 13, 36, 37]. Here, the same resonant soft-x-ray pulses also act as an active perturbation that stabilizes an otherwise inaccessible local order [4, 6, 38]. This dual role is particularly relevant for correlated materials, where spin, orbital, electronic, and lattice degrees of freedom are strongly coupled. Combining local modification by intense x-ray pulses with the element and momentum selectivity of resonant scattering provides a route to identify irradiation-stabilized competing orders in fragile quantum materials [39–41].

In summary, we have observed an XFEL-induced incommensurate order in CrAs at $\boldsymbol{q}_2$, distinct from the native helical magnetic order at $\boldsymbol{q}_1$. The induced order is resonantly enhanced at the Cr L edge, exhibits polarization-dependent resonant scattering, develops below $T^* \approx 230$ K, possesses a correlation length of approximately 4 nm, and recovers on a picosecond timescale after near-infrared excitation. These results demonstrate that intense soft-x-ray FEL irradiation can locally modify the ordering landscape of a correlated magnet

and stabilize a competing short-range order absent in pristine CrAs.

METHODS

Sample preparation

Single crystals of CrAs were grown by the Sn-flux method as described previously [42]. The crystallographic orientation was determined by back-reflection Laue diffraction. A selected crystal was mounted such that the scattering plane contained the *ac* plane, allowing access to reflections along $(0, 0, L)$. The native magnetostructural transition was verified by transport measurements, which showed a clear resistivity anomaly near 263 K, consistent with previous reports on high-quality CrAs crystals.

Synchrotron XAS and RSXS

X-ray absorption spectroscopy (XAS) and resonant soft-x-ray scattering (RSXS) measurements were performed at Beamline 20U2 of the Shanghai Synchrotron Radiation Facility. The sample was mounted on an in-vacuum four-circle diffractometer equipped with a helium-flow cryostat. Incident photon energies were scanned across the Cr $L_{2,3}$ edges with an energy resolution of approximately 0.2 eV at the Cr L_3 edge. The incident polarization was switchable between σ- and π-linear polarization. Reciprocal-space scans along $(0, 0, L)$ were performed using coupled sample and detector rotations, and scattered photons were recorded with a CCD area detector. Details of the Lorentzian fitting, integrated-intensity extraction, correlation-length estimation, and resonant-energy-profile analysis are provided in Supplementary Section II.

Scanning transmission electron microscope

Cross-sectional lamellas were prepared from the XFEL-irradiated region using focused ion beam milling. A protective carbon layer was deposited before thinning. The lamellas were thinned to approximately 100 nm at 30 kV, followed by low-voltage polishing at 2 kV. HAADF-STEM measurements were performed using a JEM-NEOARM200 transmission electron microscope operated at 200 kV.

Time-resolved RSXS

Time-resolved RSXS measurements were performed at the TXS endstation of the Shanghai soft-x-ray Free-Electron Laser. The sample was mounted on a cryogenic six-axis manipulator and cooled to approximately 29 K. Soft-x-ray FEL probe pulses were tuned near the Cr L_3 edge and were incident with horizontal π polarization. After transmission through the downstream KB optics, the photon number at the sample was estimated to be 2.75×10^{10} photons per pulse, corresponding to a peak photon fluence of 5.2×10^{14} photons cm^{-2} pulse^{-1}. The optical pump pulses had a photon energy of 1.55 eV, pulse duration of 82 fs, and fluence of 0.57 mJ cm^{-2}. The pump footprint was larger than the x-ray probe footprint, ensuring approximately homogeneous excitation within the probed region. The overall temporal resolution was 297 fs, determined from the pump-induced reflectivity change of a YAG reference. FEL pulse intensity was monitored shot by shot using gas-monitor detectors, and the time-resolved diffraction intensity was extracted from shot-by-shot ROI–GMD correlations. Details of the pulse monitoring, photon-fluence estimation, photon-energy-drift treatment, and dynamical fitting are provided in Supplementary Sections I, III, and IV.

CONFLICT OF INTEREST

The authors declare that they have no conflict of interest.

ACKNOWLEDGMENTS

This work was supported by the National Key R&D Program of China (Grant No. 2023YFA1406303, 2022YFA1403202), the National Natural Science Foundation of China (Grant Nos. 12422404, 12274085, 12404081 (Q. Jiang), 12234006 (Y. Shen and J. Zhao)), the New Cornerstone Science Foundation, the Quantum Science and Technology-National Science and Technology Major Project (Grant Nos. 2021ZD0302803, 2024ZD0300103) and the Shanghai Municipal Science and Technology Project (Grants No. 2019SHZDZX01 and No. 25DZ3008100). Resonant soft-X-ray scattering and time-resolved measurements were performed at Beamline 20U2 of Shanghai Synchrotron Radiation Facility (SSRF) and TXS endstation of Shanghai soft-X-ray Free Electron Laser (SXFEL).

AUTHOR CONTRIBUTIONS

H.X., R.P., M.Y., and D.F. conceived the project. Y.S. and J.Z. grown the single crystals. J.Y., Z.A., S.T., L.Z., Z.C., and H.X. performed synchrotron RSXS experiments. M.Y., Q.J., W.H., and J.Y. performed the time-resolved RSXS experiments and related data analysis. X.S. and collaborators performed STEM characterization. J.Y. and H.X. analyzed the synchrotron data and wrote the manuscript with input from all authors.

DATA AVAILABILITY

The data that support the findings of this study are available from the corresponding authors upon reasonable request.

[1] D. Basov, R. Averitt, and D. Hsieh, Towards properties on demand in quantum materials, Nature materials **16**, 1077 (2017).

[2] M. Buzzi, M. Först, R. Mankowsky, and A. Cavalleri, Probing dynamics in quantum materials with femtosecond x-rays, Nature Reviews Materials **3**, 299 (2018).

[3] A. Zong, B. R. Nebgen, S.-C. Lin, J. A. Spies, and M. Zuerch, Emerging ultrafast techniques for studying quantum materials, Nature Reviews Materials **8**, 224 (2023).

[4] M. Mitrano, A. Cantaluppi, D. Nicoletti, S. Kaiser, A. Perucchi, S. Lupi, P. Di Pietro, D. Pontiroli, M. Ricco, S. R. Clark, *et al.*, Possible light-induced superconductivity in k3c60 at high temperature, Nature **530**, 461 (2016).

[5] T. Kampfrath, A. Sell, G. Klatt, A. Pashkin, S. Mährlein, T. Dekorsy, M. Wolf, M. Fiebig, A. Leitenstorfer, and R. Huber, Coherent terahertz control of antiferromagnetic spin waves, Nature Photonics **5**, 31 (2011).

[6] L. Stojchevska, I. Vaskivskyi, T. Mertelj, P. Kusar, D. Svetin, S. Brazovskii, and D. Mihailovic, Ultrafast switching to a stable hidden quantum state in an electronic crystal, Science **344**, 177 (2014).

[7] P. Emma, R. Akre, J. Arthur, R. Bionta, C. Bostedt, J. Bozek, A. Brachmann, P. Bucksbaum, R. Coffee, F.-J. Decker, *et al.*, First lasing and operation of an ångstrom-wavelength free-electron laser, nature photonics **4**, 641 (2010).

[8] C. Bostedt, S. Boutet, D. M. Fritz, Z. Huang, H. J. Lee, H. T. Lemke, A. Robert, W. F. Schlotter, J. J. Turner, and G. J. Williams, Linac coherent light source: The first five years, Rev. Mod. Phys. **88**, 015007 (2016).

[9] H. Jang, H.-D. Kim, M. Kim, S. H. Park, S. Kwon, J. Y. Lee, S.-Y. Park, G. Park, S. Kim, H. Hyun, *et al.*, Time-resolved resonant elastic soft x-ray scattering at pohang accelerator laboratory x-ray free electron laser, Review of Scientific Instruments **91** (2020).

[10] M. Mitrano and Y. Wang, Probing light-driven quantum materials with ultrafast resonant inelastic x-ray scattering, Communications Physics **3**, 184 (2020).

[11] S. P. Hau-Riege, R. A. London, H. N. Chapman, and M. Bergh, Soft-x-ray free-electron-laser interaction with materials, Phys. Rev. E **76**, 046403 (2007).

[12] S. P. Hau-Riege, H. N. Chapman, J. Krzywinski, R. Sobierajski, S. Bajt, R. A. London, M. Bergh, C. Caleman, *et al.*, Subnanometer-scale measurements of the interaction of ultrafast soft x-ray free-electron-laser pulses with matter, Phys. Rev. Lett. **98**, 145502 (2007).

[13] A. Barty, C. Caleman, A. Aquila, N. Timneanu, L. Lomb, T. A. White, J. Andreasson, *et al.*, Self-terminating diffraction gates femtosecond x-ray nanocrystallography measurements, Nat. Photonics **6**, 35 (2012).

[14] Y. Shen, Q. Wang, Y. Hao, B. Pan, Y. Feng, Q. Huang, L. Harriger, J. Leao, Y. Zhao, R. Chisnell, *et al.*, Structural and magnetic phase diagram of cras and its relationship with pressure-induced superconductivity, Physical Review B **93**, 060503 (2016).

[15] W. Wu, J. Cheng, K. Matsubayashi, P. Kong, F. Lin, C. Jin, N. Wang, Y. Uwatoko, and J. Luo, Superconductivity in the vicinity of antiferromagnetic order in cras, Nature communications **5**, 5508 (2014).

[16] M. Matsuda, F. Lin, R. Yu, J.-G. Cheng, W. Wu, J. Sun, J. Zhang, P. Sun, K. Matsubayashi, T. Miyake, *et al.*, Evolution of magnetic double helix and quantum criticality near a dome of superconductivity in cras, Physical Review X **8**, 031017 (2018).

[17] H. Kotegawa, S. Nakahara, R. Akamatsu, H. Tou, H. Sugawara, and H. Harima, Detection of an unconventional superconducting phase in the vicinity of the strong first-order magnetic transition in cras using as 75-nuclear quadrupole resonance, Physical Review Letters **114**, 117002 (2015).

[18] C. Guo, M. Smidman, B. Shen, W. Wu, F. Lin, X. Han, Y. Chen, F. Wu, Y. Wang, W. Jiang, *et al.*, Evidence for triplet superconductivity near an antiferromagnetic instability in cras, Physical Review B **98**, 024520 (2018).

[19] S. Park, S. Shin, S.-I. Kim, S. Kim, C.-K. Park, J. D. Thompson, and T. Park, Tunable quantum critical point and detached superconductivity in al-doped cras, npj Quantum Materials **4**, 49 (2019).

[20] M. R. Norman, Superconductivity with a twist, Physics **8**, 24 (2015).

[21] L. Keller, J. S. White, M. Frontzek, P. Babkevich, M. A. Susner, Z. C. Sims, A. S. Sefat, H. M. Rønnow, and C. Rüegg, Pressure dependence of the magnetic order in cras: A neutron diffraction investigation, Physical Review B **91**, 020409 (2015).

[22] H. Boller and A. Kallel, First order crystallographic and magnetic phase transition in cras, Solid State Communications **9**, 1699 (1971).

[23] K. Selte, A. Kjekshus, W. E. Jamison, A. F. Andresen, J. E. Engebretsen, and L. Ehrenberg, Magnetic structure and properties of cras., Acta Chemica Scandinavica **25**, 1703 (1971).

[24] A. Kallel, H. Boller, and E. Bertaut, Helimagnetism in mnp-type compounds: Mnp, fep, cras and cras1- xsbx mixed crystals, Journal of Physics and Chemistry of Solids **35**, 1139 (1974).

[25] B. Pan, H. Xu, Y. Liu, R. Sutarto, F. He, Y. Shen, Y. Hao, J. Zhao, L. Harriger, and D. Feng, Anomalous helimagnetic domain shrinkage due to the weakening of the dzyaloshinskii-moriya interaction in cras, Physical Review B **102**, 104432 (2020).

[26] H. Jang, B. Kang, B. K. Cho, M. Hashimoto, D. Lu, C. Burns, C.-C. Kao, and J.-S. Lee, Observation of orbital order in the half-filled 4 f gd compound, Physical Review Letters **117**, 216404 (2016).

[27] S. Lovesey and S. Collins, X-ray scattering and absorption by magnetic materials. oxford series on synchrotron radiation (1996).

[28] M. Ramakrishnan, Y. Joly, Y. W. Windsor, L. Rettig, A. Alberca, E. M. Bothschafter, P. Lejay, R. Ballou, V. Simonet, V. Scagnoli, *et al.*, Crystal symmetry lowering in chiral multiferroic ba 3 tafe 3 si 2 o 14 observed by x-ray magnetic scattering, Physical Review B **95**, 205145 (2017).

[29] F. M. F. de Groot, J. C. Fuggle, B. T. Thole, and G. A. Sawatzky, 2p x-ray absorption of 3d transition-metal compounds: An atomic multiplet description including the crystal field, Phys. Rev. B **42**, 5459 (1990).

[30] F. M. F. de Groot, Multiplet effects in x-ray spectroscopy, Coord. Chem. Rev. **249**, 31 (2005).

[31] S. Watanabe, T. Nagasaki, and K. Ogasawara, Relativistic many-electron calculations of cr3+ l2, 3-edge x ray absorption near-edge structures for cr3+: α-al2o3 and α-cr2o3 and magnetic circular dichroism of cr3+ l2, 3-edge x ray absorption near-edge structures for cr3+: α-al2o3, Journal of Applied Physics **110** (2011).

[32] E. Beaurepaire, J.-C. Merle, A. Daunois, and J.-Y. Bigot, Ultrafast spin dynamics in ferromagnetic nickel, Phys. Rev. Lett. **76**, 4250 (1996).

[33] A. Kirilyuk, A. V. Kimel, and T. Rasing, Ultrafast optical manipulation of magnetic order, Rev. Mod. Phys. **82**, 2731 (2010).

[34] Y. D. Chuang, W. S. Lee, Y. F. Kung, A. P. Sorini, B. Moritz, R. G. Moore, L. Patthey, M. Trigo, *et al.*, Real-time manifestation of strongly coupled spin and charge order parameters in stripe-ordered $la_{1.75}sr_{0.25}nio_4$ nickelate crystals using time-resolved resonant x-ray diffraction, Phys. Rev. Lett. **110**, 127404 (2013).

[35] S. Johnson, R. De Souza, U. Staub, P. Beaud, E. Möhr-Vorobeva, G. Ingold, A. Caviezel, V. Scagnoli, W. Schlotter, J. Turner, *et al.*, Femtosecond dynamics of the collinear-to-

spiral antiferromagnetic phase transition in cuo, Physical review letters **108**, 037203 (2012).

[36] R. Neutze, R. Wouts, D. van der Spoel, E. Weckert, and J. Hajdu, Potential for biomolecular imaging with femtosecond x-ray pulses, Nature **406**, 752 (2000).

[37] H. N. Chapman, P. Fromme, A. Barty, T. A. White, R. A. Kirian, A. Aquila, M. S. Hunter, J. Schulz, D. P. DePonte, U. Weierstall, *et al.*, Femtosecond x-ray protein nanocrystallography, Nature **470**, 73 (2011).

[38] D. Fausti, R. I. Tobey, N. Dean, S. Kaiser, A. Dienst, M. C. Hoffmann, S. Pyon, T. Takayama, H. Takagi, and A. Cavalleri, Light-induced superconductivity in a stripe-ordered cuprate, Science **331**, 189 (2011).

[39] M. P. M. Dean, Y. Cao, X. Liu, S. Wall, D. Zhu, R. Mankowsky, V. Thampy, X. M. Chen, J. G. Vale, D. Casa, *et al.*, Ultrafast energy- and momentum-resolved dynamics of magnetic correlations in the photo-doped mott insulator sr_2iro_4, Nat. Mater. **15**, 601 (2016).

[40] M. Mitrano and Y. Wang, Probing light-driven quantum materials with ultrafast resonant inelastic x-ray scattering, Commun. Phys. **3**, 184 (2020).

[41] M. Trigo, M. Fuchs, J. Chen, M. P. Jiang, M. Cammarata, S. Fahy, D. M. Fritz, K. Gaffney, S. Ghimire, A. Higginbotham, *et al.*, Fourier-transform inelastic x-ray scattering from time- and momentum-dependent phonon–phonon correlations, Nat. Phys. **9**, 790 (2013).

[42] W. Wu, X. Zhang, Z. Yin, P. Zheng, N. Wang, and J. Luo, Low temperature properties of pnictide cras single crystal, Science China Physics, Mechanics and Astronomy **53**, 1207 (2010).

Supplementary Files

This is a list of supplementary files associated with this preprint. Click to download.

- SMforSoftxrayfreeelectronlaserpulsesstabilizeacompetingorderinhelimagnetupdated.pdf